analytical chemistry

Letter

pubs.acs.org/ac

High-Resolution Chemical Depth Profiling of Solid Material Using a Miniature Laser Ablation/Ionization Mass Spectrometer

Valentine Grimaudo,[‡] Pavel Moreno-García,[‡] Andreas Riedo,*,[†] Maike B. Neuland,[†] Marek Tulej,[†] Peter Broekmann,[‡] and Peter Wurz[†]

[†]Physics Institute, Space Research and Planetary Sciences, University of Bern, Sidlerstrasse 5, 3012 Bern, Switzerland

[‡]Department of Chemistry and Biochemistry, Interfacial Electrochemistry Group, University of Bern, Freiestrasse 3, 3012 Bern, Switzerland

ABSTRACT: High-resolution chemical depth profiling measurements of copper films are presented. The 10 μm thick copper test samples were electrodeposited on a Si-supported Cu seed under galvanostatic conditions in the presence of particular plating additives (SPS, Imep, PEI, and PAG) used in the semiconductor industry for the on-chip metallization of interconnects. To probe the trend of these plating additives toward inclusion into the deposit upon growth, quantitative elemental mass spectrometric measurements at trace level concentration were conducted by using a sensitive miniature laser ablation ionization mass spectrometer (LIMS), originally designed and developed for *in situ* space exploration. An ultrashort pulsed laser system ($\tau \sim 190$ fs, $\lambda = 775$ nm) was used for ablation and ionization of sample material. We show that with our LIMS system, quantitative chemical mass spectrometric analysis with an ablation rate at the subnanometer level per single laser shot can be conducted. The measurement capabilities of our instrument, including the high vertical depth resolution coupled with high detection sensitivity of ~10 ppb, high dynamic range $\geq 10^8$, measurement accuracy and precision, is of considerable interest in various fields of application, where investigations with high lateral and vertical resolution of the chemical composition of solid materials are required, these include, e.g., wafers from semiconductor industry or studies on space weathered samples in space research.

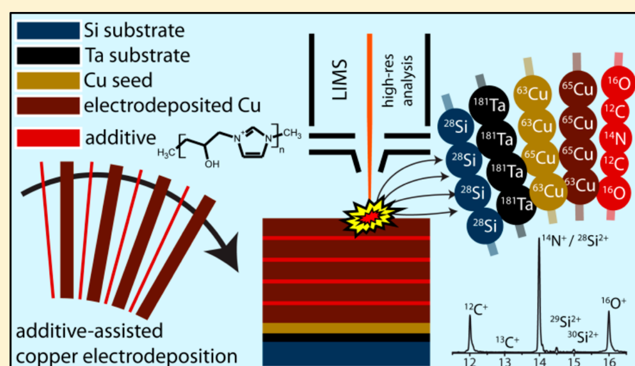

Additive-assisted Cu electroplating is a metal deposition process of high technological relevance. This process is used in the semiconductor industry for the on-chip metallization of interconnects on nonplanar (patterned) wafer surfaces with feature dimensions ranging from the sub-10 nm level (Damascene applications) up to the micrometer-scale (Through Silicon Via technology).[1,2] The presence of particular additives during the electroplating is a crucial prerequisite for the successful fill of vias and trenches on these patterned Si wafers with Cu material.[3] It is actually the nonuniform surface concentration of either suppressing (e.g., polyalkylene glycol (PAG), which is a copolymer of polyethylene glycol and polypropylene glycol, polymerizate of imidazole and epichlorohydrin (Imep), polyethylenimine (PEI)) or accelerating (e.g., bis(sodium sulfopropyl) disulfide (SPS)) additives which leads to a redistribution of the local Cu deposition velocity and thus to a so-called bottom-up fill of trenches and vias with Cu.[4−9] However, a major drawback of the use of these plating additives is their trend toward incorporation into the Cu deposit upon growth. The accumulation of contaminants in the resulting Cu film is known to significantly decelerate a desired postdeposition recrystallization that is mandatory to improve the conductivity of these Cu interconnects.[10]

To further improve the industrial process, it is therefore vital to develop analytical techniques allowing a precise quantification of the contamination level in the Cu deposit, which depends on the particular deposition parameters (electrolyte composition, current density, applied potential, etc.). One common approach to probe the contamination level is based on depth profiling techniques, e.g., secondary ion mass spectrometry (SIMS). For this purpose, the Cu films are typically deposited under galvanostatic conditions (constant deposition velocity) on planar (nonpatterned) test wafer specimens. The sputter-induced depth erosion of the sample as well as the semiquantitative characteristic of the SIMS instrument, however, rend this depth profiling technique not convenient for the investigation of additive inclusions.[11] Herein we report on a new quantitative depth profiling technique with subnanometer resolution based on laser ablation ionization mass spectrometry (LIMS).

To demonstrate the performance of our LIMS system, we particularly focus on Cu test samples that have been deposited

Received: November 25, 2014
Accepted: January 26, 2015

 © XXXX American Chemical Society

DOI: 10.1021/ac504403j
Anal. Chem. XXXX, XXX, XXX−XXX

under experimental conditions where the additives adsorb and desorb on the Cu surface in an oscillatory manner thus resulting into a layered Cu film where clean regimes in the Cu deposit are separated by horizontal boundary layers with a locally increased concentration of (additive) contaminants.[11,12]

The LIMS instrument used in this study, the miniature laser mass spectrometer (LMS), was originally developed for space research, for the *in situ* chemical analysis of planetary surfaces.[13] The measurement requirements for the LMS instrument for space research are basically the same as for many LIMS instruments in laboratory research: quantitative elemental analysis, accurate isotope analysis, high dynamic range, spatially and depth resolved mass spectrometric measurements.[14] So far, we demonstrated the LMS capabilities for highly sensitive elemental analyses,[15,16] for accurate isotope analysis,[17,18] and for 2D element images of heterogeneous surfaces.[19] Depth profiling is important in space science since samples on planetary surfaces are always affected by space weathering. That is, the rocks and soil particles have a rind of 10−100 nm that is chemically altered from the underlying bulk material, as a result of prolonged space plasma irradiation.[20] Thus, depth analysis is an important feature of *in situ* chemical composition study of material on planetary surfaces.

■ EXPERIMENTAL SECTION

Sample Preparation. For a quantitative depth profiling analysis, the mean ablation rate needs to be determined first, describing the amount of material being eroded per single laser pulse at a given laser irradiance. Test samples of well-defined thickness are required for this purpose. Therefore, we electrodeposited 10 μm-thick Cu films under galvanostatic conditions (at constant current density; J = mA/cm^2) on Cu-seeded Si-wafer coupons using an Autolab potentiostat/galvanostat (PGSTAT 128).[9,11] The blanket wafers (Hionix, BASF) were composed of a Si(100)-type substrate covered by a 500 nm thick TOx/SiO_2 dielectric layer, a 25 nm thick Ta/TaN barrier, and a terminating 100 nm thick Cu seed layer.

The basic Cu plating bath was composed of 40 g/L Cu^{2+} ($CuSO_4{\cdot}5H_2O$, Sigma-Aldrich, Steinheim, Germany), 10 g/L H_2SO_4 (VLSI selectipur 96%, BASF, Ludwigshafen, Germany) and 50 ppm of Cl (HCl 25%, for analysis, Merck, Darmstadt, Germany).

To provoke the incorporation of contaminants into the Cu deposit during growth, we carried out electrodeposition experiments in the presence of well-defined amounts of Damascene plating additives. Table 1 lists the additive packages

Table 1. Additives Used for Electrochemical Deposition of Cu on Si-Wafers

sample	used additives
S1	without additive
S2	25 ppm of SPS ($C_6H_{14}O_6S_4$) + 100 ppm PAG
S3	25 ppm of SPS + 100 ppm PEI $(C_2H_5N)_n$
S4	25 ppm of SPS + 100 ppm Imep $(C_6H_9N_2O)_n$

that were added to the respective plating bath. Sample 1 (S1) thereby serves as an internal reference electroplated deposit without any extra additives. In cases of S2−S4, we added the same amount of 25 ppm of SPS (Raschig, Ludwigshafen, Germany). These samples, however, differ in the chemical nature of the polymeric suppressor additives used. S2 was electroplated in the presence of 100 ppm PAG (BASF, Ludwigshafen, Germany), S3 in the presence of 100 ppm PEI (BASF, Ludwigshafen, Germany), and S4 in the presence of 100 ppm Imep (BASF, Ludwigshafen, Germany). All samples experienced a 1 week room temperature (RT) self-annealing before they were analyzed by LIMS depth profiling.

Laser Ablation Ionization Mass Spectrometer. Mass spectrometric studies were conducted by using our miniature reflectron-type time-of-flight (TOF) laser mass spectrometer (LMS). The details of the technical design and principles of operation of LMS are described in previous publications.[15−19] Therefore, only a brief overview of the instrument and measurement principles are given in the following.

An ultrashort pulsed laser system ($\tau \sim 190$ fs, $\lambda = 775$ nm, laser pulse repetition rate $\leq$1 kHz) is used as an ablation ionization source.[17] The laser system is located outside the vacuum chamber, and an optical system is used for beam shaping and delivery to the mass spectrometer located within the vacuum chamber. Laser pulse energy, laser pulse repetition rate, and number of laser pulses are fully controlled by the interface of the laser system. A doublet lens on top of the mass analyzer is used to focus the laser beam through the system on the sample surface (laser ablation crater with a diameter of about 14 μm). The laser focus, and thus the sample surface, is positioned close to the entrance of the ion-optical system, about 1 mm away. A high-resolution x−y−z micro translation stage with a position accuracy of about 2 μm is used for the positioning of samples relative to the mass spectrometer. Only positively charged ions, generated by the interaction of the laser pulse with the sample surface, can enter the mass analyzer. Entering the mass analyzer the ions are accelerated, focused, and confined with an ion optical system into the instrument, pass the field free region, and are reflected by the ion mirror back toward the detector system.

The ions arrive at the detector system sequentially in time according to their mass to charge (m/z) ratio (TOF principle), where they produce electrical signals. Two high speed ADC systems (8 bit vertical resolution, up to 4 GS/s) are used for the acquisition of the electric signal, the TOF spectrum (length of 20 μs). Once the measurement campaign is accomplished, the TOF spectra can be converted to mass spectra (m/z) by using the relation $(m/z)(t) = a(t - t_0)^2$, where a and t_0 are calibration constants.[15]

Typically, an entire measurement campaign consists of up to several thousands of single laser shots mass spectra. The current measurement setup allows acquiring and saving single laser shot mass spectra on the host computer and its real time visualization on a screen. Custom-made analysis software, written in MATLAB, is used for subsequent data analysis.

Measurement Procedure. Laser irradiances in the range of 2.7−6.8 TW/cm^2 (0.8−2 μJ/pulse, laser ablation crater diameter $\sim$14 μm) were applied in this study on the four different samples (S1−S4, see Table 1). Each measurement was conducted on a fresh and untreated sample location. The continuous acquisition of mass spectra in each measurement campaign (defined laser irradiance on defined sample and location) was stopped once the Si signal coming from the ablation of the SiO_2 substrate was observed. The depth profile for each element was acquired by analyzing the temporal evolution of the signal intensity of the certified element/isotope in the TOF spectra (for more details see ref 17). With the knowledge of the Cu layer thickness and number of applied laser shots the mean ablation rate per single laser shot can be derived (more details are given in the following section).

DOI: 10.1021/ac504403j
Anal. Chem. XXXX, XXX, XXX−XXX

■ RESULTS AND DISCUSSIONS

Figure 1 shows the mean ablation rate of Cu per single laser shot deduced from measurement campaigns conducted on the four different samples S1−S4 by applying different laser irradiances. The mean ablation rate shows a logarithmic dependence with laser pulse energy. No significant differences in the mean ablation rate can be observed by using none (S1) or the different additives (S2−S4) for electrochemical Cu deposition. At higher laser pulse energies, an increase in ablation rate is observed, as expected. Subnanometer vertical resolution is achieved at the lowest laser irradiances which is, to the best of our knowledge, the highest resolution ever achieved by a LIMS system and about 1 decade better as shown recently by Cui et al.[21] For example, by applying ∼0.9 μJ per laser pulse, we obtained a mean ablation rate of ∼0.3 nm of Cu, which would correspond to a mean ablation rate of 1.35 atomic layers, assuming Cu(111) orientation. We notice, however, that only pulse energies above ∼0.9 μJ enable a stable ablation process. Comparable quantitative and sensitive chemical analysis of elements/isotopes with abundances in the sample material in the range of femtogram to picogram was shown recently by Zhang et al. and Gao et al. by using an orthogonal buffer-gas-assisted LIMS system with a spatial resolution of about 40−80 μm.[22,23]

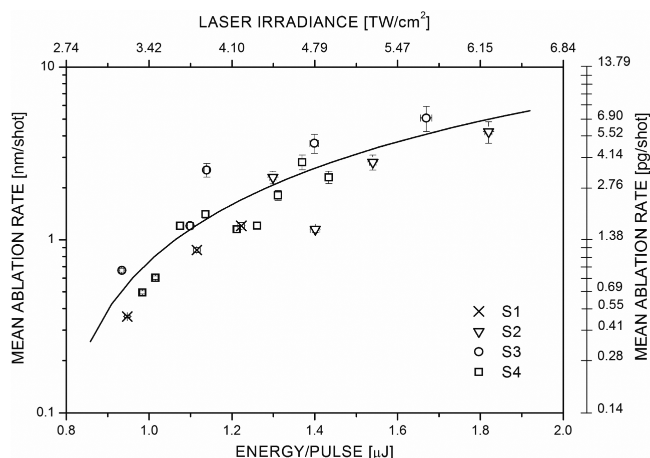

Figure 1. Mean ablation rate for single laser shots of Cu as a function of the laser pulse energy for the four different samples (S1−S4, see Table 1). The solid line is a trend line and is only given to guide the reader's eye.

Figure 2 shows the depth profile analysis of S2, where the additives SPS and PAG were used for the galvanostatic Cu deposition (see Table 1). The Si substrate is encountered after about 6410 single laser shots, which corresponds to a mean ablation rate of Cu of about 1.56 nm/shot.

After the ablation of the Cu film, we observe the signal from the Ta layer and the rise of the Si signal from the substrate. The Ta layer with a thickness of only 25 nm can be easily resolved (see the inset of Figure 2). Knowing the thickness of the Ta layer, we infer that the ablation rate of Ta is about half of that of Cu at the same laser pulse energy. For both Ta and Si, an initial increase of the ion yield prior to the main ablation peak at the interface is observed (for Ta around 6435, for Si around 6450 single laser shots). The nature of this effect (observed in all our measurements) is not fully understood at present. The observation of this transient effect can be related to a change of the ablation conditions at the interface between two different materials and will be explored in more details in forthcoming studies.

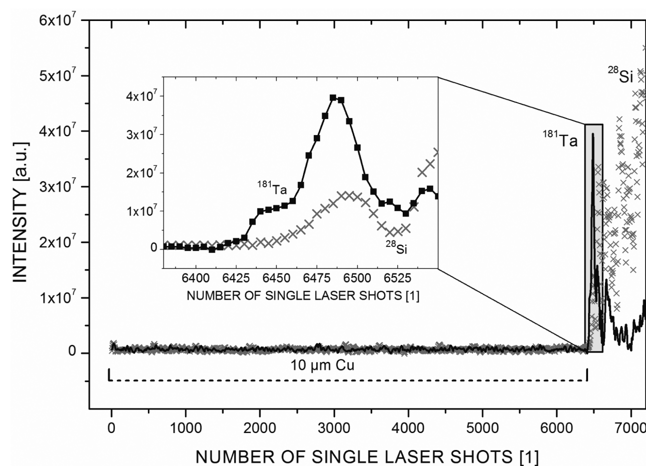

Figure 2. Depth profile measurements of S2 at a laser irradiance of ∼3.7 TW/cm^2.

Single laser shot campaign and the high detection sensitivity of the LMS instrument allow the chemical analysis of thin layers of any solid material with high resolution. An example of the depth profiling capabilities of the LMS instrument is illustrated in Figure 3, which shows a section of the depth profile of S4. This range, which is representative of the whole depth profile, is chosen to make it easy for the reader to discern the fine structure of the chemical depth profiling. The deposition of the Cu film is interrupted by thin layers of contaminants because of quasi-periodic fluctuations of the Cu deposition rate in the presence of SPS and Imep additives in the electrolyte.[11,12] Figure 3 shows these oscillations evidenced by the clear anticorrelation between the Cu and the C, N, and O signals, which are the major contaminant elements. The mean full width at half-maximum (FWHM) for these narrow contaminant layers was calculated to be approximately 22 nm, which would correspond to about 100 Cu(111) atomic layers. The depth profile of the contaminants in S4 shows an average incorporation periodicity of 600 nm, which is indicated in Figure 4 by vertical bars in gray. The total incorporation abundance was observed to vary between 99.8% and 0.2%

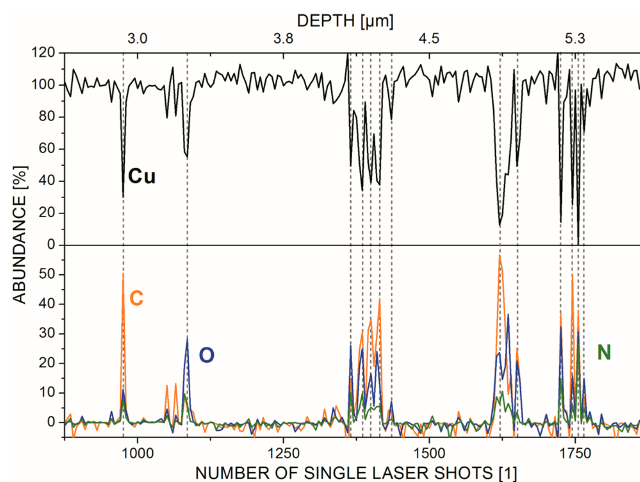

Figure 3. Section of depth profile of Cu and the major contaminants C, N, and O for S4.

DOI: 10.1021/ac504403j
Anal. Chem. XXXX, XXX, XXX−XXX

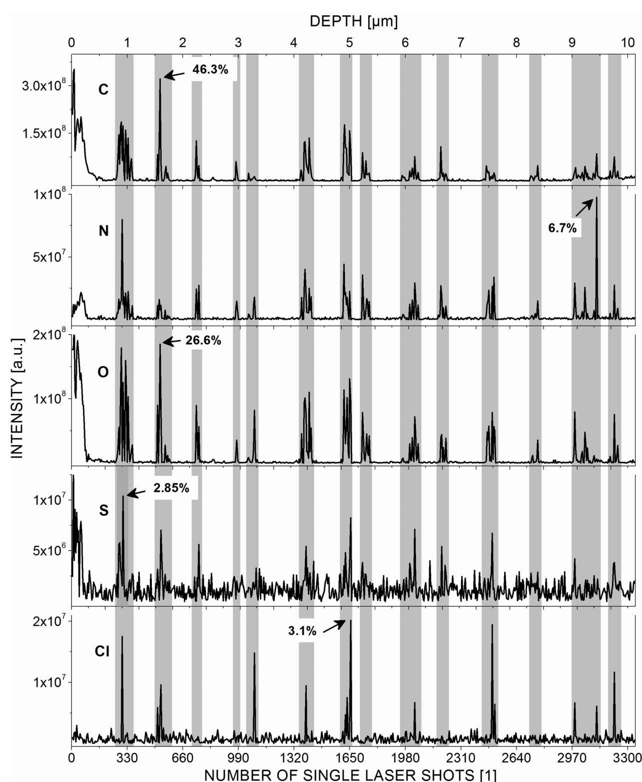

Figure 4. Depth profiles of S4 of all relevant elements of the contamination layers (C, N, O, S) and from the electrolyte (Cl, S).

relative to the deposited Cu amount. The contaminants C, N, and O show over the whole range identical fluctuations. This periodicity partially holds for S and Cl. However, the missing features for these two later elements (namely, those of Cl in Figure 4), coupled to the results of ref 11, lead us to conclude that Cl (and probably S) do not always coincide with the Imep embedment. Additionally, the concentration of these species is significantly lower than that of the major impurities. This is why, we suggest that their embedment into the copper matrix do not necessarily correlates with the appearance of C, N, and O signals and that their incorporation might be accounted for a different chemical process, e.g., interaction between electrolyte and electrode.

The suppressing additive Imep (polymerizate of imidazole and epichlorohydrin, see Table 1) induces a characteristic potential oscillation during the galvanostatic Cu deposition, which is attributed to a periodic degradation and restoration of the active suppressor film at the Cu/electrolyte interface.[11] Cross-sectional focused ion beam (FIB) micrographs of these Cu films have shown sharp horizontal grain-boundary lines, where the Cu recrystallization is inhibited. The formation of these boundaries was observed to correlate with the presence of the suppressor ensemble and their frequency is dependent on the applied current density during deposition. Earlier SIMS measurements revealed concentration modulation of contaminants within the Cu deposit, which are assigned to a periodic embedding behavior of the suppressor additive. However, the low vertical resolution of these SIMS depth profiles, attributed to sample roughening during the sputtering process, prevents the exact local assignment of contaminants within the Cu deposit.[11] To understand under which conditions these additives get incorporated into the deposit, we need to investigate the chemical composition at the boundary sites. 3D quantitative imaging of the Cu film is provided by the LMS instrument. In contrast to SIMS, negligible sample roughening is obtained during the laser ablation process. The preservation of the layered structure during the measurements gives rise to the observation of sharp intensity peaks in the depth profile of S4 (see Figure 3). Since the synergistic interaction of Imep and SPS is responsible for the oscillations in the Cu deposition, it is expected that their components will contribute significantly to the chemical composition of the contamination layering when the Cu deposition is degraded.

Figure 4 shows the quantitative analysis of the depth profiles of all relevant elements of the contamination layers (C, N, O, S), which is compatible with the inclusion of Imep and SPS. In addition, traces from the electrolyte (Cl, S) are also found in the contamination layer. All these species show a concentration modulation that is perfectly in phase (see gray vertical lines in Figure 4) and which is opposite to the Cu signal, i.e., a clear anticorrelation between the Cu signal and the contaminants (Figures 3 and 4). In accordance with the oscillatory nature of the chemical deposition process, we observe that the incorporation of the suppressing ensemble inhibits the Cu deposition at the growth interface.

■ CONCLUSIONS

With the help of well-defined Cu layers on Si wafers we could calibrate the depth analysis of our LMS instrument. On the basis of this depth calibration, we measured and analyzed layered samples produced by a galvanostatic Cu deposition process. Because of the synergistic interaction of Imep and SPS dissolved in the plating bath, the analyzed samples bear a well-known oscillatory structure of the deposited materials with thick Cu and thin contaminant layers. Because of the high depth resolution of the LMS instrument we could resolve each of the contaminant layers of approximately 22 nm thickness and determine quantitatively their chemical composition. The high depth resolution of the LMS measurement, which is to our knowledge the best vertical resolution ever measured with a LIMS system, enables us to study in detail the chemical nature of the contaminant layers.

■ AUTHOR INFORMATION

Corresponding Author

*E-mail: andreas.riedo@space.unibe.ch. Phone: +41 31 631 44 49.

Notes

The authors declare no competing financial interest.

■ ACKNOWLEDGMENTS

This work is supported by the Swiss National Science Foundation.

■ REFERENCES

(1) Dubin, V. M.; Alkolkar, R.; Cheng, C. C.; Chebiam, R.; Fajardo, A.; Gstrein, F. *Electrochim. Acta* **2007**, *52*, 2891−2897.
(2) Gagnard, X.; Mourier, T. *Microelectron. Eng.* **2010**, *87*, 470−476.
(3) Andricacos, P. C.; Uzoh, C.; Dukovic, J. O.; Horkans, J.; Deligianni, H. *IBM J. Res. Dev.* **1998**, *42*, 567−573.
(4) Akolkar, R.; Landau, U. *J. Electrochem. Soc.* **2004**, *151*, C702−C711.
(5) Akolkar, R.; Landau, U. *J. Electrochem. Soc.* **2009**, *156*, D351−D359.

(6) Moffat, T. P.; Bonevich, J. E.; Huber, W. H.; Stanishevsky, A.; Kelly, D. R.; Stafford, G. R.; Josell, D. J. *Electrochem. Soc.* **2000**, *147*, 4524−4535.
(7) Moffat, T. P.; Wheeler, D.; Edelstein, M. D.; Josell, D. *IBM J. Res. Dev.* **2005**, *49*, 19−36.
(8) Moffat, T. P.; Wheeler, D.; Kim, S. K.; Josell, D. J. *Electrochem. Soc.* **2006**, *153*, C127−C132.
(9) Broekmann, P.; Fluegel, A.; Emnet, C.; Arnold, M.; Roeger-Goepfert, C.; Wagner, A.; Hai, N. T. M.; Mayer, D. *Eletrochim. Acta* **2011**, *56*, 4724−4734.
(10) Zhou, J.; Reid, J. D. *ECS Trans.* **2007**, *2*, 77−92.
(11) Hai, N. T. M.; Odermatt, J.; Grimaudo, V.; Krämer, K. W.; Fluegel, A.; Arnold, M.; Mayer, D.; Broekmann, P. *J. Phys. Chem. C* **2012**, *116*, 6913−6924.
(12) Hai, N. T. M.; Lechner, D.; Stricker, F.; Furrer, J.; Broekmann, P. *ChemElectroChem.* **2015**, DOI: 10.1002/celc.201402427.
(13) Rohner, U.; Whitby, J.; Wurz, P. *Meas. Sci. Technol.* **2003**, *14*, 2159−2164.
(14) Wurz, P.; Abplanalp, D.; Tulej, M.; Iakovleva, M.; Fernandes, V. A.; Chumikov, A.; Managadze, G. *Sol. Sys. Res.* **2012**, *46*, 408−422.
(15) Riedo, A.; Bieler, A.; Neuland, M.; Tulej, M.; Wurz, P. *J. Mass Spectrom.* **2013**, *48*, 1−15.
(16) Tulej, M.; Iakovleva, M.; Leya, I.; Wurz, P. *Anal. Bioanal. Chem.* **2011**, *399*, 2185−2200.
(17) Riedo, A.; Neuland, M.; Meyer, S.; Tulej, M.; Wurz, P. *J. Anal. At. Spectrom.* **2013**, *28*, 1256−1269.
(18) Riedo, A.; Meyer, S.; Heredia, B.; Neuland, M. B.; Bieler, A.; Tulej, M.; Leya, I.; Iakovleva, M.; Mezger, K.; Wurz, P. *Planet. Space Sci.* **2013**, *87*, 1−13.
(19) Neuland, M. B.; Meyer, S.; Mezger, K.; Riedo, A.; Tulej, M.; Wurz, P. *Planet. Space Sci.* **2014**, *101*, 196−209.
(20) Noguchi, T.; Nakamura, T.; Kimura, M.; Zolensky, M. E.; Tanaka, M.; Hashimoto, T.; Konno, M.; Nakato, A.; Ogami, T.; Fujimura, A.; Abe, M.; Yada, T.; Mukai, T.; Ueno, M.; Okada, T.; Shirai, K.; Ishibashi, Y.; Okazaki, R. *Science* **2011**, *333*, 1121−1124.
(21) Cui, Y.; Moore, J. F.; Milasinovic, S.; Liu, Y.; Gordon, R. J.; Hanley, L. *Rev. Sci. Instrum.* **2012**, *83*, 093702.
(22) Zhang, B.; He, M.; Hang, W.; Huang, B. *Anal. Chem.* **2013**, *85*, 4507−4511.
(23) Gao, Y.; Lin, Y.; Zhang, B.; Zou, D.; He, M.; Dong, B.; Hang, W.; Huang, B. *Anal. Chem.* **2013**, *85*, 4268−4272.

DOI: 10.1021/ac504403j
Anal. Chem. XXXX, XXX, XXX−XXX